A bottom-up emission estimate for the 2022 Nord Stream gas leak: derivation, simulations and evaluation

Rostislav Kouznetsov[1], Risto Hänninen[1], Andreas Uppstu[1], Evgeny Kadantsev[1], Yalda Fatahi[1], Marje Prank[1], Dmitrii Kouznetsov[2], Steffen Noe[3], Heikki Junninen[4], and Mikhail Sofiev[1]

[1]Finnish Meteorological Institute, Helsinki, Finland
[2]University of Electro-Communications, Tokyo, Japan
[3]Estonian University of Life Sciences, Tartu, Estonia
[4]University of Tartu, Estonia

Correspondence: Rostislav Kouznetsov (Rostislav.Kouznetsov@fmi.fi)

Abstract. A major release of methane from the Nord Stream pipelines occurred in the Baltic sea on 26 September 2022. Elevated levels of methane were recorded at many observational sites in northern Europe. While it is relatively straightforward to estimate the total emitted amount from the incidents (around 330 kt of methane), the detailed vertical and temporal distributions of the releases are needed for numerical simulations of the incident. Based on information from public media and basic

5   physical concepts, we reconstructed vertical profiles and temporal evolution of the methane releases from the broken pipes, and simulated subsequent transport of the released methane in the atmosphere. Since we used pure-methane assumption, the inventory total amounts to 290 kt of methane.

      The emission rates were calculated with a numerical solution of a problem of a gas leak from a half-opened pressurized pipe. Initial vertical distribution of the released gas was derived from a parametrization for an injection height of buoyant plumes,

10   and validated with a set of large-eddy simulations by means of UCLALES model.

      The estimated emission source was used to simulate the dispersion of the gas plume with the SILAM chemistry transport model. The simulated fields of the excess methane led to noticeable increase of concentrations at several carbon-monitoring stations in the Baltic Sea region. Comparison of the simulated and observed time series indicated an agreement within a couple of hours between timing of the plume arrival/departure at the stations with observed methane peaks. Comparison of absolute

15   levels was quite uncertain. At most of the stations the magnitude of the observed and modelled peaks was comparable with natural variability of methane concentrations. The magnitude of peaks at a few stations close to the release was well above natural variability, however the magnitude of the peaks was very sensitive to minor uncertainties in the emission vertical profile and in the meteorology used to drive SILAM.

      The obtained emission inventory and the simulation results can be used for further analysis of the incident and its climate

20   impact. They can also be used as a test case for atmospheric dispersion models.

1 Introduction

A major release of methane from the Nord Stream pipelines 1 and 2 occurred at the bottom of the Baltic sea on 26 September 2022 as a result of explosions at both lines. At the moments of the blasts, both pipes were filled with pressurized methane but no gas pumping was happening. Over the following days, methane escaped from the damaged pipes to the atmosphere.

25   Natural gas mining and transport through pipelines are considered among the safest means of energy transport. Over the period 1800 - 2018, less than 300 serious accidents have been documented worldwide, which is, for instance, 4 times less than in oil transport, 8 times less than in the coal industry, and 10% lower than accidents count in wind energy (Kim et al., 2021). In the standard practice, accidents in the energy sector are categorized in terms of fatalities and property damage, which are documented by the authorities (e.g., Pipeline and Hazardous Materials Safety Administration in the US). Other

30   parameters, such as the amount of natural gas released to the atmosphere, are rarely considered. However, in the Nord Stream the atmospheric release was one of important characteristics of the incident. To put it into a large-scale context, one can note the annual release of methane from the US gas production and distribution system: 13 (+2.1/-1.6, 95% confidence interval) Tg CH_4/year in 2015, i.e. 2.3% of the total production in that year (Alvarez et al., 2018). This number includes both releases from normal and abnormal operations and exceeds the official US EPA methane emission in 2015 (8.1 Tg/y, EPA, 2017) by

35   5 Tg/y or 60%. Alvarez et al. suggested that the disagreement is partly due to accidental releases, which are not accounted for in the official EPA inventory. They estimated the gas transportation-only contribution to the CH_4 emission as 1.8 Tg/y (both normal and abnormal operations), whereas the US EPA regular-operation estimate is 1.4 Tg/y (normal operations). Comparison of these numbers suggests that the annual accidental losses in the US gas transport system are ∼400 Gg/y (EPA, 2017). The release from one of three breached Nord Stream pipes was estimated to be 115 Gg (Sanderson, 2022), over 30% of the above

40   annual leaks due to accidents on the US pipelines (over 5 mln km of the total length) but accounts for around 0.14% of the global annual methane emissions from the oil and gas industry (Sanderson, 2022). Therefore, albeit extremely large for a single case, the Nord Stream leaks alone could hardly have a measurable impact on the global scale (Chen and Zhou, 2022).

Long atmospheric lifetime of methane and large radiative effect makes it a major greenhouse gas Tollefson (2022). Since it also has very low deposition velocity and solubility (100 times less soluble in water than CO_2), its release at virtually any

45   height leads to large-scale distribution. However, methane is flammable at mixing ratios of 5 to 15 volume percent (Zabetakis, 1964) and in large concentrations can be very hazardous due to oxygen deprivation (e.g. Duncan, 2015). Therefore, emergency management of large releases, similar to the one considered in this study, requires detailed knowledge of the release temporal and vertical distribution, and evolution of resulting surface concentrations.

Methane density is about half of the air density, therefore a concentrated release of methane creates a powerful buoyant

50   plume, which raises in the atmosphere similarly to an overheated plume from a major fire. Numerous (semi)empirical models and parameterisations have been developed for estimating the equilibrium height and vertical profile of injection of buoyant plumes into the air. However, these models were developed for industrial stacks and provide unrealistic results with very powerful buoyant releases or releases that take place over extended area (Sofiev et al., 2012; Li et al., 2023). Models more
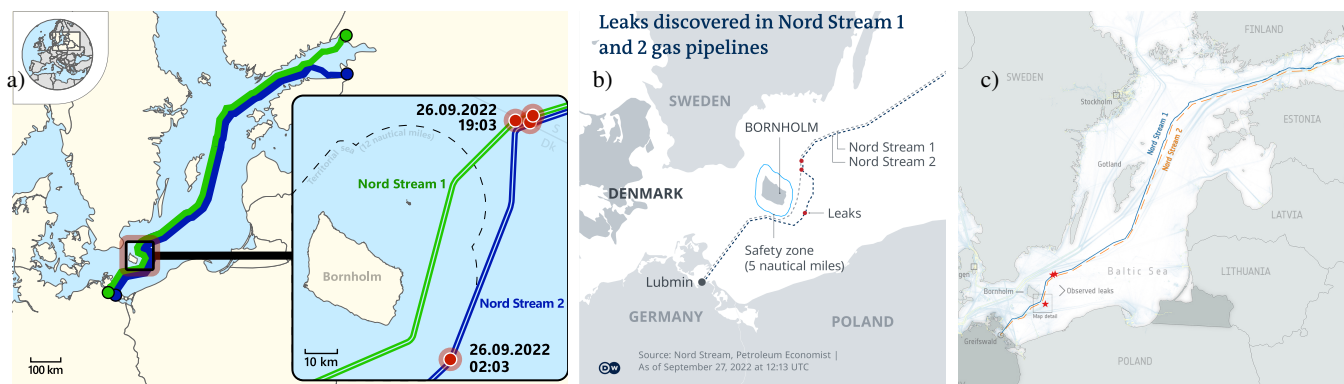
Figure 1. Maps of the Nord Stream gas leaks from various sources. a) Wikimedia https://upload.wikimedia.org/wikipedia/commons/e/e1/Nord_Stream_gas_leaks_2022.svg (CC BY-SA 4.0), b) Deutsche Welle (https://www.dw.com/en/denmark-sweden-view-nord-stream-pipeline-leaks-as-deliberate-actions/a-63251217), c) European Space Agency (ESA, https://www.esa.int/ESA_Multimedia/Images/2022/10/Nordstream_pipeline_map_with_shipping_traffic).

suitable in such conditions have been developed for vegetation fires (Freitas et al., 2007; Sofiev et al., 2009, 2012; Rémy et al., 2017).

The accidents at the Nord Stream pipelines have been extensively reported in mass media and various Internet resources. Many mutually-contradicting facts about the pipeline, leak locations and their intensity have been published. Even the locations and number of leaks have been specified differently by different sources (Fig 1).

There have been several publications analysing the gas releases from the pipes. The total amount of about 110 kt of methane per pipe (around 330 kt in total) can be calculated on a back of envelope if one assumes the initial pressure in the broken pipes of 105 Bar and knows their sizes. The amount varies depending on the assumption on the natural gas composition and the initial gas pressure. These calculations were performed in several studies. Jia et al. (2022) assumed that there were two pipes destroyed, so reported 230 kt of total methane released. Sanderson (2022) reported 115 kt from the NS2 pipe. The worst-case scenario considered by the Danish environmental agency amounts to 500 kt (https://ens.dk/en/press/possible-climate-effect-gas-leaks-nord-stream-1-and-nord-stream-2-pipelines, accessed on 15.8.2023), which is probably based on the design pressure of the pipeline, rather than on the pressure when the pipeline is idle.

The total released amount has been analyzed also by inverse techniques. The Norwegian Institute for Air Research reported total emissions in the range between 56 and 155 kt of methane (https://www.nilu.com/2022/10/improved-estimates-of-nord-stream-leaks/,accessed on 15.8.2023). Jia et al. (2022) reported 220 ± 30 kt, which nicely coincides with their bottom-up estimate. None of these studies considered the effect of methane buoyancy on the plume injection or initial release height.

The goals of the current paper are: (i) to construct a self-consistent and physically feasible picture of the event, (ii) to calculate the bottom-up time-resolving emission of methane from the Nord Stream broken pipes, (iii) to estimate the vertical extent of the plume injection and its evolution, (iv) to calculate the plume dispersion in the atmosphere during several days since the

release using Finnish emergency and atmospheric composition model SILAM, (v) to evaluate the resulting simulations against observational data.

The paper is structured as follows. The next section describes the models and the observational data sets used to evaluate the inventory. Section 3 formulates a mathematical model for temporal evolution of the leak intensity. Section 4 formulates an approach to evaluate the injection height for the buoyant methane plume. Section 5 summarizes the parameters of the pipelines and the gas leaks available from media and literature and formulates the emission source for the Nord Stream 2022 gas leaks, and compares the injection profile obtained from the parametrization to the vertical distribution simulated with a Large-Eddy Simulation model. Section 6 describes the simulations of the methane dispersion from the leaks and the results of their comparison against the observation stations.

2   Modelling tools and measurement data

2.1   SILAM chemistry-transport model

To simulate the plume dispersion we have used an atmospheric chemistry transport model (CTM) SILAM (https://silam.fmi.fi). The model features mass-conservative non-diffusive Eulerian advection scheme (Sofiev et al., 2015), and has been used in many applications for research, operational forecasting and emergency-response purposes. The model can operate at various resolutions: starting from sub-kilometer resolution in a limited-area mode, to much several-degree resolution in global mode. Feasible vertical resolutions normally start from around 10 m near the surface to thicker several-kilometer layers in free troposphere and stratosphere.

Being an offline CTM, SILAM requires a pre-computed set of meteorological fields to drive the transport and transformation processes. SILAM can consume meteorological fields from many numerical weather-prediction models (NWP), and climate models. For the present study we use operational global forecasts of the European Center for Medium-Range Forecasts (ECMWF) obtained with the Integrated Forecasting System (IFS), and forecasts from the unperturbed member of the Mesoscale Ensemble Prediction System (MEPS) for Nordic countries. MEPS is based on the Harmonie meteorological model. From both models, series of hourly forecasts with the shortest available lead time were used. The ECMWF forecast was taken with the resolution of 0.1×0.1 degrees, and the MEPS forecasts were used at the original resolution of 2.5 km.

SILAM allows for several types of meteorology-dependent emission sources, including dynamic injection height for wildland fires Sofiev et al. (2012). For the current study, the fire plume-rise module has been interfaced to the point-source module, enabling injection of large buoyant plumes. For such sources, the buoyancy flux is provided along with the emission rate, and the former is used to evaluate the injection height range.

2.2   UCLALES large eddy simulator

The applicability of the fire plume rise module of SILAM for the current task was evaluated by comparing to fine scale simulations of the buoyant plume made with the large eddy simulator UCLALES (Stevens et al., 1999, 2005; Stevens and Seifert,

105 2008). The methane emissions were included to UCLALES as volumetric flux from the underlying surface. The horizontal distribution of the emission flux from the surface was assumed normal, 99% (3 standard deviations) fitting in a circular area with 500 m diameter. The formula for virtual temperature that is used for computing the vertical acceleration due to buoyancy was amended to account for methane mixing ratio in the grid cell.

UCLALES simulations were initialized with temperature, humidity and wind profiles and surface variables taken from
110 the same ECMWF forecasts used for SILAM simulations. Simulations were made in a 5 km high domain spanning 18 km in downwind and 6 km in crosswind direction. The domain was selected to be large enough to extend beyond the vertical and cross-wind spread of the plume and thus not interfere with these processes, and long enough in downwind direction for the plume rise process to finish and the resulting final height become analyzable. The simulations were made with 50 m horizontal and 10 m vertical resolution and time step with maximal length of 1 second, automatically reduced if required by
115 flow conditions for stability of the UCLALES numerical schemes.

2.3 Observational data

To validate our simulation results, we use observational time series of atmospheric methane concentrations obtained by the Integrated Carbon Observation System (ICOS) network, https://icos-cp.eu (accessed 30.11.2022). We use hourly time series of in-air volume mixing ratio of methane over several dozens of stations in Europe. Many stations have tall towers with the
120 observations at several heights up to few hundred meters above the surface.

We show the data from five ICOS stations: Finnish Utö station (UTO) located in the Baltic sea (Hatakka and Laurila, 2022), Swedish Norunda (NOR) and Hyltemossa (HTM) stations (Lehner and Mölder, 2022; Heliasz and Biermann, 2022), Norwegian Birkenes (BIR) and Zeppelin (ZEP) stations (Lund Myhre et al., 2022a, b).

In addition to the ICOS stations, we have used data from several Finnish (Kilkki et al., 2015) and Estonian (Noe et al., 2015;
125 Luts et al., 2023; Hõrrak et al., 2000) sites. Despite the stations using very similar protocols to ICOS, they are currently not a part of the ICOS network.

In the figures below, the ICOS time series are marked with their three-letter codes and corresponding height in meters. Other stations have been marked with a two-letter code of the country and a three-letter abbreviation of the station name. The complete list of the stations, their locations and references for the ICOS time series used can be found in the Supplementary
130 material.

3 Equations for a methane leak from a half-open pipe

To estimate the leak discharge as a function of time, let us consider an idealized system: a long smooth round pipe of inner diameter D and length L ($L \gg D$), which is closed at both ends and filled with a pressurized gas of initial density ρ_0. At the moment t_0 one end of the pipe is opened and the gas starts leaking.

135   The evolution of the gas velocity $v(x,t)$ and density $\rho(x,t)$ along the pipe can be described by the equation of motion:

$$\rho \frac{\partial v}{\partial t} = -\frac{\partial p}{\partial x} - \frac{\rho v^3}{2D|v|} f, \tag{1}$$

and the continuity equation:

$$\frac{\partial \rho}{\partial t} = -\frac{\partial(\rho v)}{\partial x}. \tag{2}$$

The first term at the rhs of Eq. 1 describes the acceleration of the gas due to the pressure gradient along the pipe, the second

140   term describes the turbulent drag. The dimensionless drag coefficient f depends on the flow regime. The relevant velocity for

the flow ranges from ten meters per second, to the speed of sound $(450\,\mathrm{m/s})$, and the kinematic viscosity of methane for the

pressure range of $10 - 100$ bar can be approximated as $\nu = 15 \times 10^{-6}\,\mathrm{m^2/s} \cdot \frac{\rho_a}{\rho}$, where ρ_a is the methane density at standard

conditions. Reynolds number $Re = vD/\nu$ of the flow exceeds 10^6 but is less than $4 \cdot 10^7$. At such Reynolds numbers the Blasius

formula is applicable:

145    $$f = (100\,Re)^{-1/4}. \tag{3}$$

To get a complete system of equations for $\rho(x,t)$ and $v(x,t)$, one needs also an equation of state that connects pressure

and density of the gas. Since the pipe is submerged in water the process of gas expansion can be considered isothermal at

temperature $T = 278\,\mathrm{K}$ (Kniebusch et al., 2019). The ideal-gas equation of state:

$$p(x,t) = \frac{R}{\mu}\rho(x,t)T, \tag{4}$$

150   where R is the universal gas constant ($R \simeq 8.3\,\mathrm{J\,K^{-1}\,mol^{-1}}$), and μ is the molar mass of the gas ($\mu = 0.016\,\mathrm{kg\,mol^{-1}}$), does

not describe methane at the relevant pressure range. In particular, it predicts some 20% lower density of methane at 100 Bar

than experimental values reported by Mollerup (1985). Therefore we use the more sophisticated van der Waals equation:

$$p(x,t) = \frac{R}{\mu}\left(\frac{1}{\rho(x,t)} - \frac{b}{\mu}\right)^{-1} T - \frac{a}{\mu^2}\rho^2(x,t), \tag{5}$$

where a and b are gas-specific van der Waals constants, describing the effects of finite volume of a gas molecule, and the

155   effects of inter-molecular attraction. For the study we use the values of $a = 0.21\,\mathrm{Jm^3/mol^2}$, $b = 4.31 \times 10^{-5}\,\mathrm{m^3/mol}$. Note

that the value of a differs from the one suggested by Poling et al. (2001) ($a = 0.2303\,\mathrm{Jm^3/mol^2}$), since our value fits better

experimental data on methane density, e.g. by Mollerup (1985) up to $15\,\mathrm{MPa}$.

The initial and boundary conditions corresponding to the pipe are

$$\rho(x,0) = \rho_0, \tag{6}$$

160    $$v(x,0) = 0, \tag{7}$$

$$v(0,t) = 0, \tag{8}$$

$$\rho(L,t) = \rho_{\mathrm{out}}, \tag{9}$$

where ρ_0 and ρ_{out} are the density of gas corresponding to the initial pressure p_0 inside the pipe and to the pressure at the open end of the pipe p_{out}.

165   Breaching a pressurized pipe at an intermediate point is equivalent to the simultaneous opening of the one end of two shorter pipes on either side from the breach.
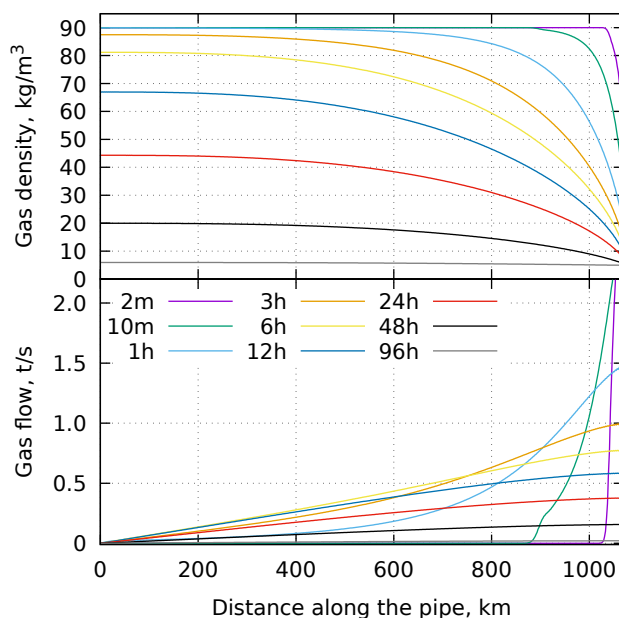
Figure 2. The along-pipe profiles of the density (upper panel) and the flow rate (lower panel) for different times (in minutes/hours, as indicated in the legend) after opening the pipe end for the pipe length of 1080 km.
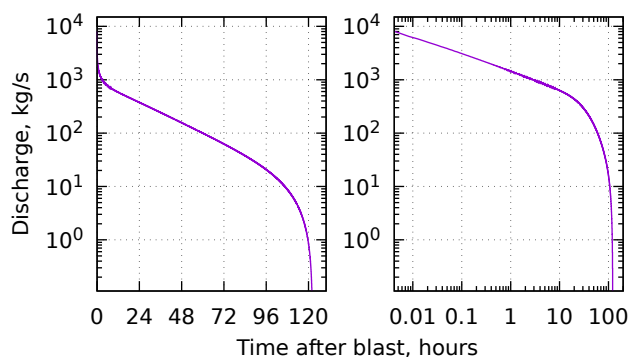
Figure 3. The gas discharge rate as a function of time after opening the pipe end for the same case as in Fig. 2 with linear (left) and logarithmic (right) time axis.

To illustrate the evolution of the gas distribution within a pipe initially pressurized with methane after one end has been opened, consider a 1080-km pipe of 1.153 m inner diameter at the initial pressure of 105 Bar and outside pressure of 7 Bar. Figure 2 shows the simulated profiles of the gas density and the gas flow along the pipe at various times after one end has been opened. The evolution of the flow in the pipe has two stages: one immediately after opening when the distortion propagates towards the closed end of the pipe, and after that almost linear flow profile along the pipe when flow is limited by the turbulent drag inside the pipe. These regimes are clearly seen also in the evolution of the discharge rate at the open end of the pipe (Fig.3). In the beginning the flow behaves as a power function of the time, and after that it starts an exponential decay. Once the flow gets slow enough so the drag is no longer significant, the remaining gas flow ceases quickly.

4   Injection height

Methane is almost twice lighter than the air. Massive injection of methane from the surface produces a buoyant plume that raises upwards and mixes out with the surrounding air losing its buoyancy. There has been a number of various models and parametrisations developed for evaluating a buoyant plume rise from industrial sources (e.g. Briggs, 1984). However, these empirical formulas appeared inaccurate for wide-area highly-buoyant sources, for which alternative solutions were proposed. In particular, a dedicated semi-empirical parameterization was suggested and evaluated for plumes from vegetation fires by Sofiev et al. (2012). Input variables for that approach are derived in this section.

The primary characteristic of buoyant plumes in plume-rise parametrisations is buoyancy flux (Venkatram and Wyngaard, 1988, (eq. 3.11 there)):

$$F_{\mathrm{b}} = F_{\mathrm{v}} g \frac{\Delta \rho}{\rho_{\mathrm{a}}}, \tag{10}$$

where F_{v} is a volumetric flux of a source (in m^3/s), g is acceleration due to gravity, $\Delta \rho$ is the difference between ambient air density $\rho_{\mathrm{a}} \simeq 1.2 \, \mathrm{kg/m^3}$ and the released gas density $\rho_{\mathrm{g}} \simeq 0.69 \, \mathrm{kg/m^3}$. It is straightforward to convert a methane discharge at the surface F_{m} (in kg/s) to the buoyancy flux:

$$F_{\mathrm{b}} = F_{\mathrm{m}} g \frac{\Delta \rho}{\rho_{\mathrm{a}} \rho_{\mathrm{g}}}. \tag{11}$$

For methane in standard conditions, the conversion coefficient $g \frac{\Delta \rho}{\rho_{\mathrm{a}} \rho_{\mathrm{g}}} \simeq 6 \, \mathrm{m^4/kg/s^2}$.

The parametrisation for plume injection heights for wildland fires Sofiev et al. (2012) uses the Fire Radiative Power (FRP) of a fire as a measure of its intensity. According to Wooster et al. (2005), FRP constitutes about 20% of the total combustion energy, competing with convective energy loss, latent heat release, and heat conductivity losses to soil. In the same work, heat conductivity to soil was suggested to be barely 5% of the total energy, thus leaving 75% of the total combustion energy distributed between sensible and latent heat releases, the former being the dominant fraction. These estimates corroborate with some works (e.g. Kremens et al., 2012), but look rather conservative in comparison with others (e.g. Ferguson et al., 2000). Admitting significant uncertainties in the relation between FRP and convective power, all studies agree that they differ by a factor of a few times at most. Since the formula of Sofiev et al. (2012) involves cubic root of FRP, one can assume that for a

fire the fractions of its power spent for radiation and for creating buoyancy are approximately equal. Then the equivalent FRP can be expressed in terms of the buoyancy flux.

200   The buoyancy of some volume of methane at temperature T_0 is equivalent to the buoyancy the same volume of air with a temperature T_{eff}:

$$T_{\text{eff}} = T_0 \frac{\rho_{\text{a}}}{\rho_{\text{g}}}. \tag{12}$$

This T_{eff} is analogous to the virtual temperature that is often used for buoyancy calculations with water vapour. Then the power needed to produce the overheated air plume of the same buoyancy as the release of the gas is:

205    $$\text{FRP} = F_{\text{m}} c_{\text{p}} T_0 \left(\frac{\rho_{\text{a}}}{\rho_{\text{g}}} - 1 \right), \tag{13}$$

where c_{p} is the specific heat capacity of air at constant pressure. At standard conditions the conversion factor to get the equivalent FRP for a methane release is $\sim 1.9 \times 10^5 \, \text{J/kg}$, which is more than two orders of magnitude smaller than the specific energy of the released gas if it was burnt ($5.6 \times 10^7 \, \text{J/kg}$).

Therefore, injection of methane at the surface at a rate of $1 \times 10^4 \, \text{kg/s}$, as in the beginning of the release shown in Fig 3, is

210   equivalent to a 2-GW fire. It is of the same order of magnitude as the most powerful fire considered by (Freitas et al., 2007), much higher than any realistic industrial sources. A smoke plume from such a fire, depending on weather conditions raises due to own buoyancy up to a few kilometres (Sofiev et al., 2012).

5   Quantifying the emission source

5.1   Reported locations, and timelines of the leaks

215   Each of the Nord Stream 1 and 2 pipelines consists of two pipes. The locations of the leaks from the pipes reported by the Danish Marine Authority are shown in Fig. 4ab. The locations of the Nord Stream 1 and a part of the Nord Stream 2 pipelines as reported by the EMODnet human activities database (https://www.emodnet-humanactivities.eu, last access 9.12.2022) are shown with solid lines. A part of the Nord Stream 2 pipeline missing from the database is sketched with a dashed line that connects the West-most point of NS2 pipeline in the database, the leak site NS2A, and the destination point of the pipeline.

220   A blast at the Nord Stream 2 pipeline was detected by a seismometer by the Geological Survey of Denmark at Bornholm island at 02:03 CEST (00Z) on 2022-09-26, and similar data were reported by several seismic stations in the region (https://www.geus.dk/om-geus/nyheder/nyhedsarkiv/2022/sep/seismologi, last access 9.12.2022). Soon after that the Nord Stream 2 pipeline's operators saw a sudden pressure drop in one of the pipes, from 105 bar to 7 bar (Sanderson, 2022), and a Danish F-16 interceptor discovered a gas leak at the location of the seismic wave origin (NS2A in Fig. 4a). On the same day, the area

225   around the location was closed by the Danish Marine Authorities for all types of vessels with the Navigational warning NW-230-22. The bubbling at the water surface at the location had been detected for several days after the blast with various satellite and airborne observations. On 1.10.2022 Danish Energy Agency reported that according to the Nord Stream 2 operator the
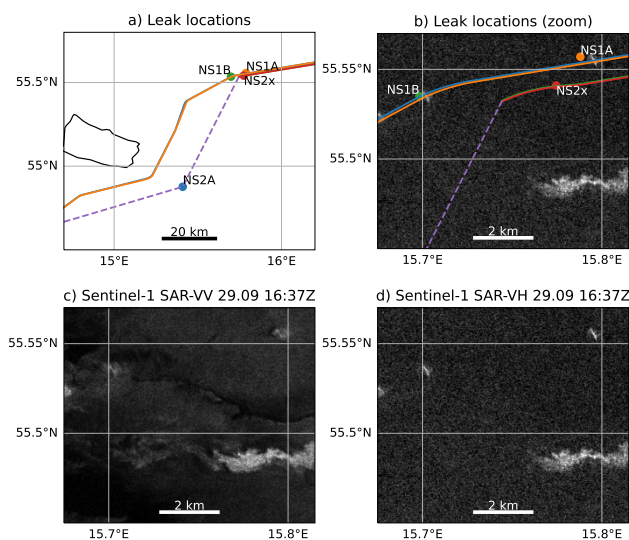
Figure 4. The locations of the gas leaks near the island of Bornholm reported by the Danish Marine Authority, and the Nord Stream pipeline (a), zoom plotted over the Sentinel-1 Synthetic-Aperture Radar backscatter acquired on 2022-09-29 at 16:36:54Z in VH polarization (b), and the same radar image in VV (c) and VH (d) polarizations. The lighter areas on the radar images indicate a disturbed water surface. The Sentinel-1 data were acquired from ESA via https://scihub.copernicus.eu.

pressure in the damaged Nord Stream 2 pipe stabilized and the gas leakage from the pipe ceased (https://apnews.com/article/russia-ukraine-putin-united-states-germany-business-afebd99d298ac72192acfeabfe384609)

230   A series of blasts at the Nord Stream 1 pipeline was detected by the same seismometers around 19:03 CEST (17Z) on 2022-09-26. According to the Navigational warning NW-235-22 by the Danish Marine Authorities, three leaks have been discovered: NS1A, NS1B, and NS2X in Fig. 4ab. The leaks NS1A, NS1B were recorded by several satellite and airborne observations during several days following the blasts. The leaks stopped on 2.10.2022 (https://sverigesradio.se/artikel/nord-stream-1-har-slutat-att-lacka-gas). We could not find any information on further leak detections at the NS2X site. The

235   location NS2X corresponds to the Nord Stream 2 pipeline. At the same time, one of the two Nord Stream 2 pipes stayed intact (https://www.reuters.com/business/energy/gazprom-lowers-pressure-undamaged-part-nord-stream-2-pipe-denmark-says-2022-10-05/), and the leak from the NS2A site continued long after 2022-09-26, therefore we conclude that NS2X was, probably reported by a mistake.

The key input needed to evaluate the amount released from the pipelines is the initial pressure in the pipes at the mo-

240   ment of rupture. Besides the aforementioned 105 bar, we could find an image of a pressure gauge seen at the landfall facility of the Baltic Sea gas pipeline Nord Stream 2 in Lubmin, Germany, September 19, 2022 (reuters.com/business/energy/gazprom-lowers-pressure-undamaged-part-nord-stream-2-pipe-denmark-says-2022-10-05) that shows 95 bar. Therefore we suggest that the accuracy of the release estimates based on the available pressure figures should be around 10-15%.

Table 1. Nord-Stream gas pipe and blast parameters assumed for the simulations

Pipe inner diameter D	1.153 m [a]
Pipe Length L	1224 km [a]
Initial pressure P_0	105 bar [b]
Water pressure at the blast point	7 bar [b]
NS2A leak	started 2022-09-26, 00Z, 54.877N,15.410E [c]
NS1A leak	started 2022-09-26, 17Z, 55.535N,15.698E[d]
NS1B leak	started 2022-09-26, 17Z, 55.557N,15.788E[d]
NS2X leak	started 2022-09-26, 17Z, 55.53N,15.6983E[d], assumed false detection

[a]Nord Stream AG (2013)

[b]Sanderson (2022)

[c]Navigational warning NW-230-22 by Denmark marine authority https://nautiskinformation.soefartsstyrelsen.dk

[d]Navigational warning NW-235-22 by Denmark marine authority https://nautiskinformation.soefartsstyrelsen.dk

5.2 The emission source
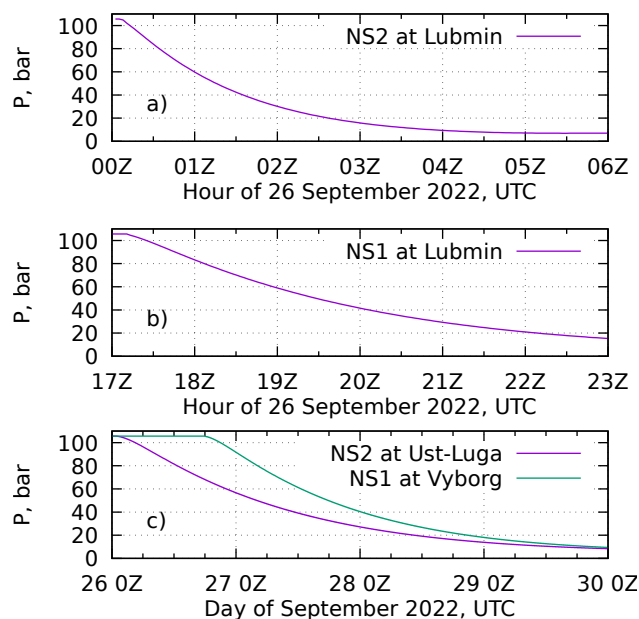
Figure 5. Pressure evolution at the landfall facilities of the Nord Stream pipelines during the leak events, according to our calculations.

245   The gas discharge from each leak can be considered as a sum of two flows from the half-opened pipes on either side of the leak. For the NS2A leak, we take the lengths of the pipe segments equal to 150 km and 1080 km, and for both NS1 leaks -
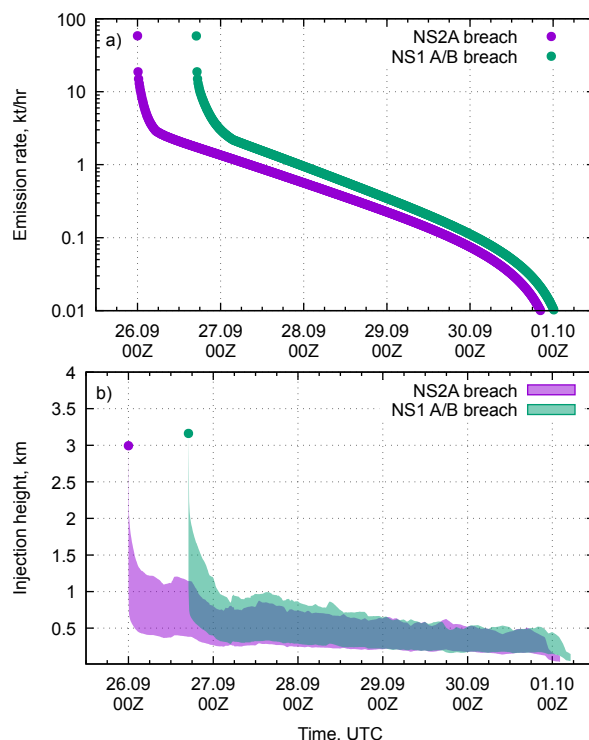
Figure 6. The simulated emission rates (a) and injection heights (b) from the breached pipelines.

230 km and 1000 km, respectively. The system of equations derived in Section 3 was evaluated for these four pipe lengths with the parameters summarized in Table 1.

There is an uncertainty about the pressure in the Nord Stream 1 pipelines. The Danish energy authority reported 165 Bar and 103 Bar for NS1 and NS2 lines respectively (https://twitter.com/Energistyr/status/1576888899288256514). The figure for NS2 agrees well with the data of Sanderson (2022). The figure for NS1 is close to the design pressure of the pipeline (170 Bar, http://www.nord-stream.com/en/the-pipeline/facts-figures.html, accessed on 04.11.2011), which is hardly consistent with the statement from the same tweet that the pressure has been lowered in the pipelines by the moment of incident. Since NS1 and NS2 have very similar characteristics, we consider 105 Bar as a reliable estimate of the pressure for both pipelines by the moment of the incident.

The temporal evolution of the pressure at the landfall facilities of the pipelines calculated for the parameters in Table 1 is given in Fig 5. The figure could be directly compared to the readings of the pressure gauges at the landfall facilities. The plot was sent to the Nord Stream AG on 16 Nov 2022 with a request for comments, however no reply had been received by the moment of the paper submission.

260   The gas discharge rates resulting from the solution of the above equations for both pipelines can be seen in Fig. 6. Both pipelines produce the same starting discharge rate, as this rate is fully determined by the pipe size and the initial pressure. The NS2A shows more rapid decrease of the rate and then stabilizes after the shorter part of the pipe A (200 km) has been drained. Then the longer end (1000 km) was gradually draining. The breaches of NS2 pipes happened closer to the middle of the pipe, therefore the initial decrease of the discharge for them is slower, but the total duration of the discharge is shorter.

265   The injection heights for the releases evaluated with the one-step procedure suggested by Sofiev et al. (2009) are given in Fig. 6b. The initial phase of the release produces a plume up to 3.5 km tall, which then quickly decreases down to approximately 1 km.

5.3   Validating the injection heights
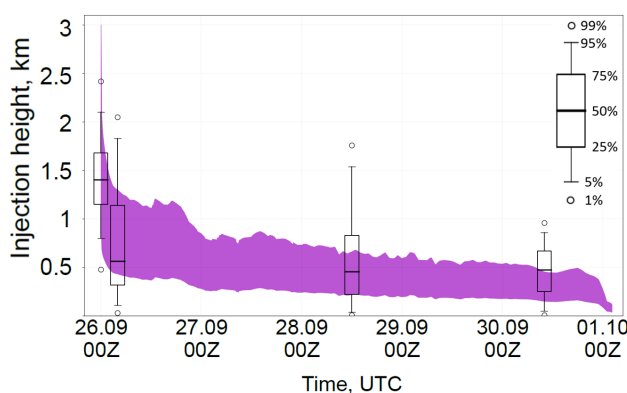
Figure 7. Comparison of the plume height parameterization with UCLALES simulations for NS2A breach. Purple – parameterization, boxes – LES simulations.

To ensure the applicability of the parametrisation for fire plumes (Sec. 4) to the methane releases we simulated the rise
270   of the buoyant plume with the large eddy simulator UCLALES. We selected 4 periods of the NS2A breach to simulate for comparison: the beginning of the release with the maximum release rate and the moments when the release rate had reduced to 1000, 100 and 10 kg/s (9.26 00:00, 9.26 4:00, 9.28 12:00 and 9.30 10:00 respectively). The LES was initialized with meteorological profiles of the selected times from ECMWF forecasts and allowed to run until the methane tracer crossed the domain downwind boundary. The rising of the plume was assumed complete far enough downwind that the vertical wind
275   component no longer correlated with the methane mixing ratio and the height of the plume between that spot and a location 15 km downwind from the release was analyzed.

Fig 7 shows the comparison of the LES simulated plume heights (box plots) with the fire plume parameterization (purple). The plume heights computed by the two methods agree reasonably well. In both cases only the initial release peak is strong enough to inject most of the methane to the free troposphere above the boundary layer (664 meters according to ECMWF
280   forecast). For the later weaker releases the LES predicts part of the methane reaching much higher altitudes than the parame-

terization. However, the models agree that majority of methane stays within the boundary layer (902 m, 490 m and 680 m for the second, third and fourth case) and there is good overlap for where most of the plume is located. The disagreement in the lower part comes from the LES freely mixing the methane through the boundary layer while the parameterization has fixed plume bottom at 1/3 of the top height. The observed differences are not expected to cause major changes in the large scale model, as the boundary layer mixing will occur there in limited time. Thus, the skill of the fire plume parameterization seems sufficient for predicting the rise of buoyant gas plumes.

One uncertainty in the LES simulations is the width of the area where the gas is emitted from the sea surface. In the main simulations the release is assumed to be distributed normally within 500 m circle. We conducted sensitivity studies varying this diameter from 100 to 1000 m for the highest release case. We found very limited sensitivity to this parameter - while the narrow emission produces somewhat narrower plume, the mean height of the plume stays practically the same (see Supplementary Material).

6 Simulating the methane dispersion from the NS leaks

With the emission source defined in the above sections, we simulated the methane dispersion for ten days following the release start. Besides the emission sources with plume rise we have used several fixed vertical profiles to evaluate the sensitivity of the simulations to the injection height. The simulations used rotated lon-lat grids closely matching the input meteorological grids. To evaluate the sensitivity of the simulations to the spatial resolution we made three sets of the simulations: VHires at $0.025° \times 0.025°$ grid, HiRes at $0.1° \times 0.1°$ grid and LoRes at $0.4° \times 0.4°$ grid. The former was driven with Harmonie meteorological model, whereas the latter two were driven with the same set of the IFS meteorological model (sec.2). For each resolution, a set of vertical injection profiles were simulated: 0–50 m, 0-500 m, 0–1500 m, 0-5000 m, and a dynamic vertical profile FRP described in Section 4. The latter injects uniformly into an elevated layer with bounds controlled by the buoyancy flux and meteorological conditions. In all simulations the same temporal profiles of emissions were used.

According to the simulations, during the period from 26.9. to 5.10.2022 the methane plume has hit many of the ICOS stations that reported data during that period. For most of them the observed variations of methane were well within the range of usual variability of the methane mixing ratios, so one could not unequivocally detect the signal originating from Nord Stream solely from the observed time series. However, if plotted in the same scale with modelled time series the peaks originating from the Nord Stream leaks can be relatively well identified.

To illustrate the results of the simulations, we have selected six stations with clearly visible signal. Fig. 8 shows four panels of timeseries for each station: observed methane content, and modelled methane excess from the three simulations. The simulations did not have any background methane. Colors correspond to observation heights for each station. The line style shows different vertical distribution of the emission. Wherever possible we kept the same vertical scale among the three panels (all stations in Fig 8 except for EE-SMR). The time series for the remaining ICOS and few non-ICOS methane-monitoring sites in Finland and Estonia can be found from supplementary materials.
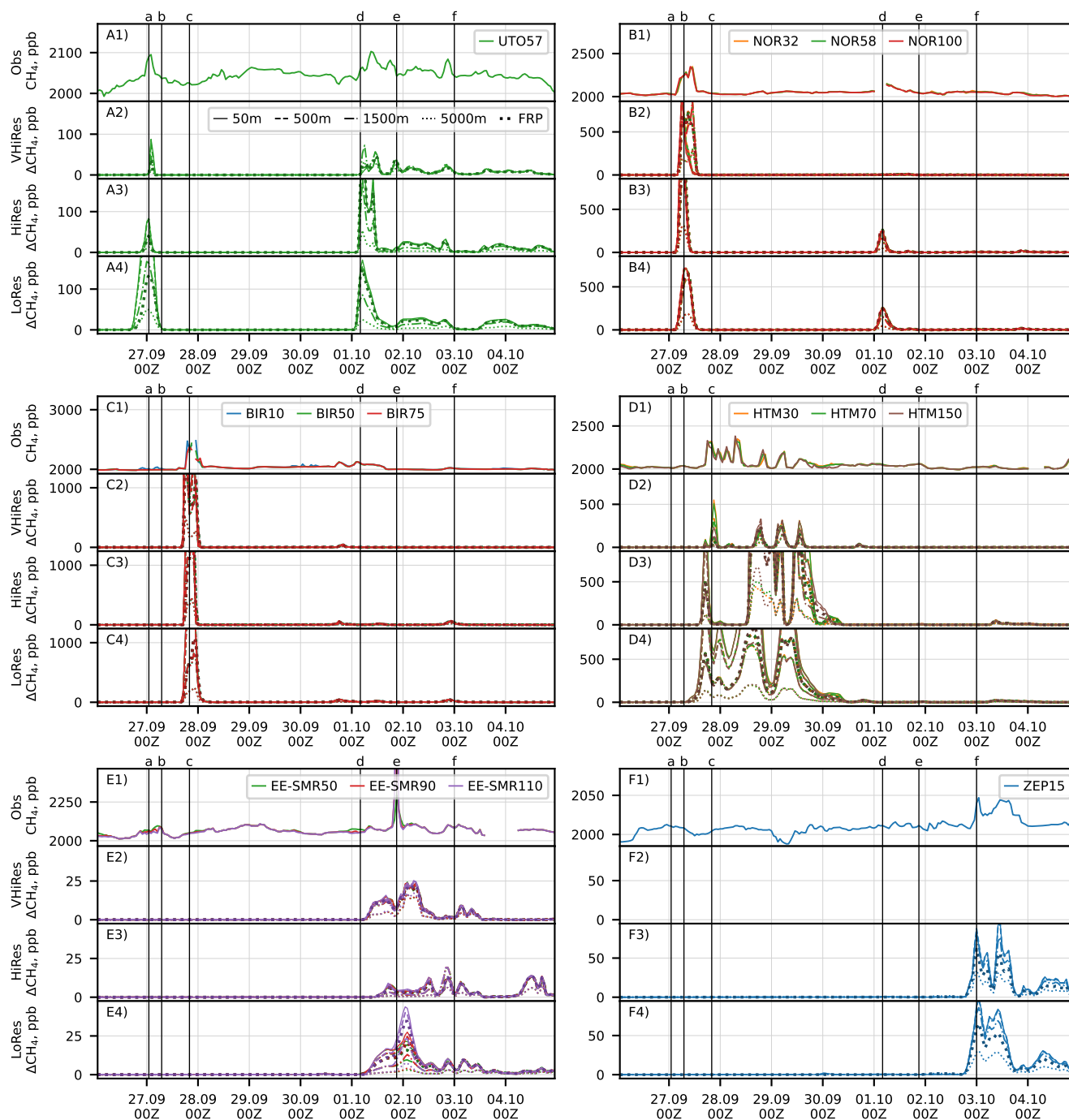
Figure 8. Timeseries of methane mixing ratio observed at six selected stations after the pipeline rupture, and corresponding timeseries simulated with three different resolutions for several vertical profiles of the release. Each group of panels corresponds to a station. The panels in each group are (top-down) for observations, and model with 0.02°, 0.1°, 0.4° resolution. Measurement heights are coded with colours, and emission heights are with line styles. Vertical lines mark the moments shown in Figs. 9–11
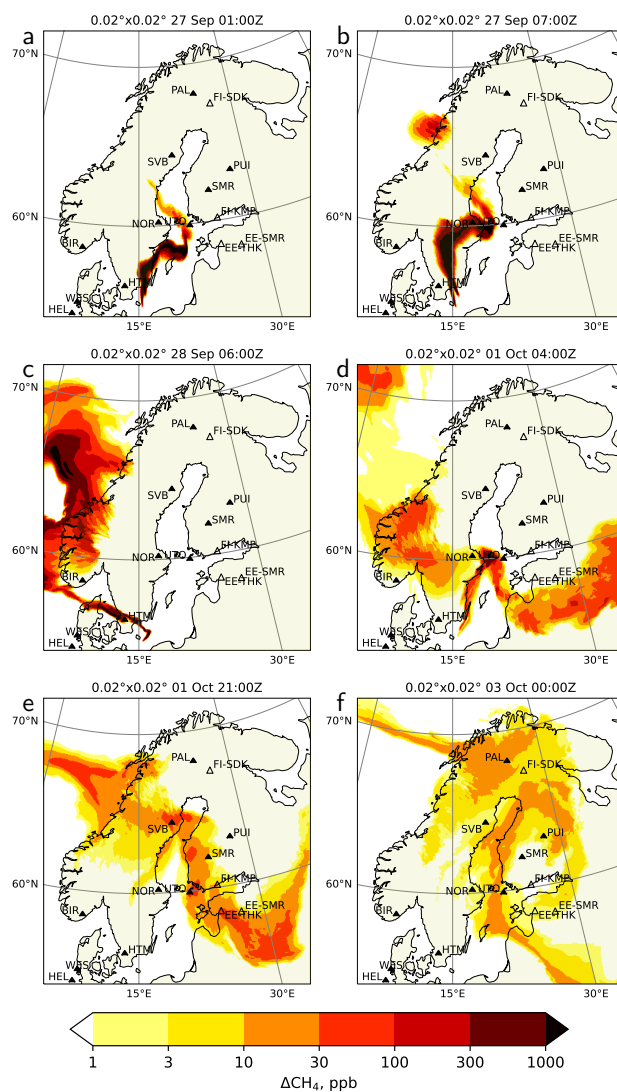
Figure 9. Snapshots of near-surface methane excess simulated at $0.02°$ resolution with SILAM driven with Harmonie meteorological fields for FRP injection profile (VHiRes setup). The panels correspond to the moments marked with vertical lines in Fig. 8.
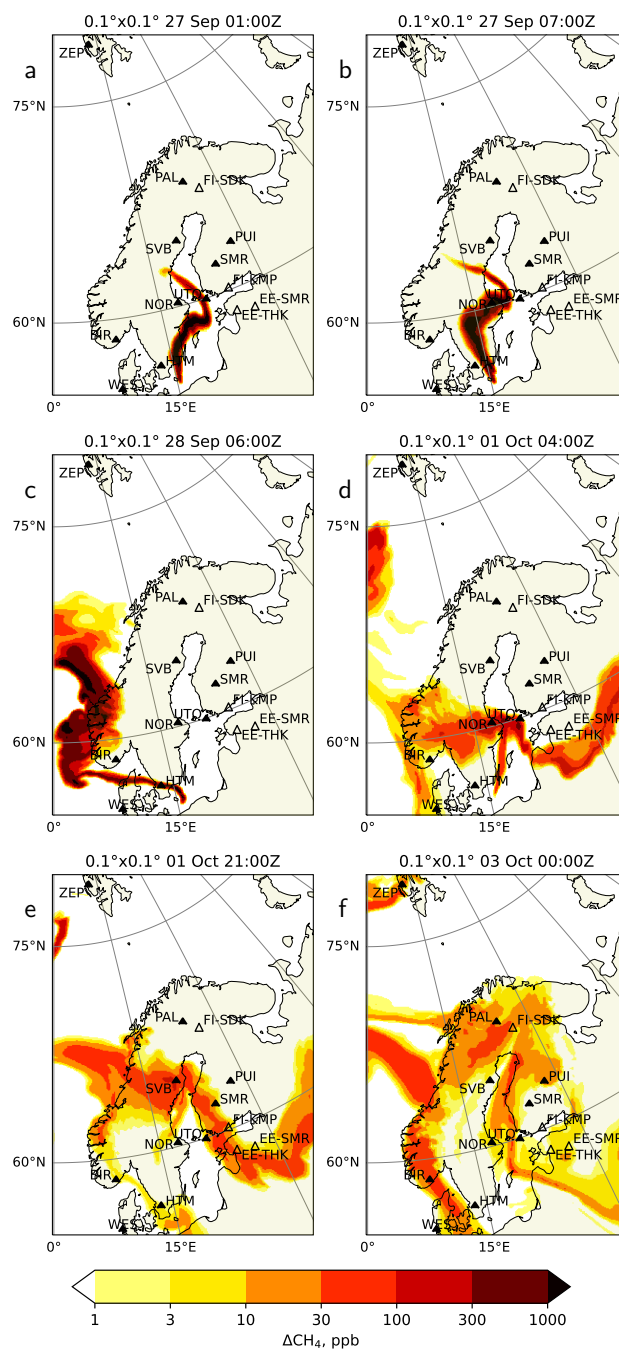
Figure 10. Same as in Fig. 9 but for 0.1° simulation driven with IFS meteorology (HiRes setup)
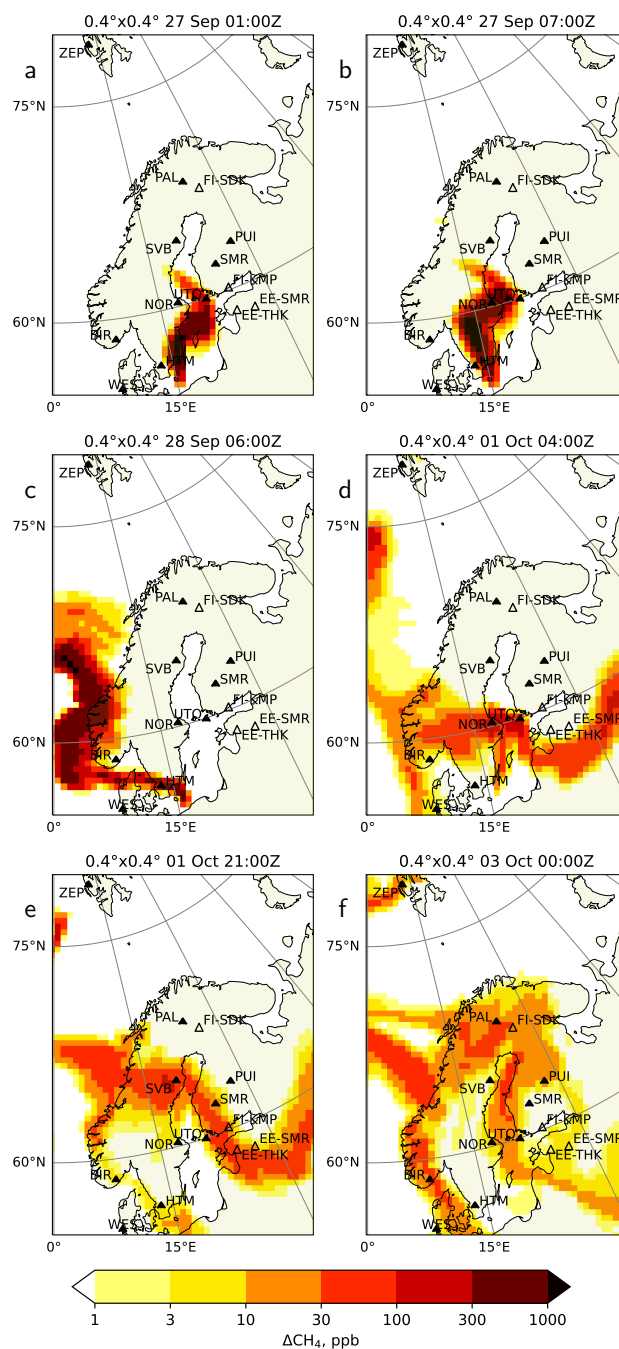
Figure 11. Same as in Fig. 9 but for 0.4° simulation driven with IFS meteorology (LoRes setup)

Six moments were selected in the time series to illustrate the spatial distribution of the simulated methane plume and its relative position to the stations. The selected moments are marked with vertical lines and letters at the top of the panels with observations in Fig 8. The maps of near-surface methane mixing ratio for the selected moments are shown in the corresponding panels in Fig. 9, Fig. 10, and Fig. 11. The ICOS stations are shown with filled symbols and three-letter codes, and other stations have two-letter country prefixes. Full list of the station data and references to them can be found from supplementary materials.

The earliest detection of the plume happened at the Utö station (UTO) located in the Baltic sea (Fig 8Ax) around midnight 27.09. (Figs 9a, 10a, and 11a). The timing of the peak is in good agreement between the observation and all simulations. In all simulations, the plume touched the station without crossing it, therefore the magnitude of the peak both in observations and simulations was strongly influenced by fine details of the plume location. The VHires and HiRes simulations produce narrower peaks than LoRes ones. The magnitude of the peak for HiRes simulations was well reproduced for the fixed injection heights in the range of 500-1500 meters, and with the dynamic injection profile. LoRes simulations clearly overestimate the peak, especially for lower injection height (reached 350 ppb). The peak originates from early-stage high-altitude injection.

There is also a nice correspondence between the measurement and modelled evolution of the time series during 1.10. and 2.10., except for a large peak during the first half of 1.10 in lower-resolution simulations. During that time the station was at the edge of the plume (see Figs 9b, 10b, and 11b), where slight uncertainties of the plume location lead to large differences in simulated concentrations.

The Norunda ICOS station (NOR) in Sweden (Fig 8Bx) has three measurement heights, which reported very similar methane mixing ratios during the simulated period. In the morning 27.9. the plume arrived at the station by showing a clear increase of methane by about 300 ppb (see Figs 9b, 10b, and 11b). The simulations show notably larger peak of up to 3500 ppb for near-surface emission scenario in HiRes case, while the peak magnitude for 5-km injection height has about right magnitude. In the VHires simulation both the shape and the magnitude of the observed peak were best reproduced with fixed 0–5000m injection profile. This indicates that the FRP injection height could be too low at the beginning of the releases. There is a gap in the measurement data corresponding to the arrival of the second peak (1.10 04Z), probably caused by the overly conservative automated quality control of the observational data. The second peak is not visible for the VHires simulation since the plume was at higher elevation (see Figs 9d, 10d, and 11d). The timings of both peaks were nicely captured by the model.

The ICOS Birkenes station (BIR) in Norway (Fig 8Cx) has detected a major peak just before midnight 28.9. Similar to NOR, the observations have a gap during the peak. The peak simulated with FRP scenario (1300 ppb for VHires and HiRes, and 800 ppb on LoRes) is stronger than the measured one, showing that the injection height was slightly underestimated, again pointing to over-conservative injection height for the FRP scenario. The simulation resolution did not have a major effect on the peak timing since the plume was already wide enough when it swiped over the station (see Figs 9c, 10c, and 11c).

During two days starting from ~12Z 27.09, the plume was meandering near the Hyltemossa ICOS station (HTM) in Sweden (Fig 8Dx) resulting in an oscillating pattern in observations. The plume was narrow (see Figs 9c, 10c, and 11c), so a slight change in wind direction resulted in large change in methane concentrations at the station. The magnitude and timing of some of the observed peaks were nicely captured by the VHires simulation, since it could make sufficiently narrow plumes, and the

Harmonie meteorology reproduced the land-sea circulation well. For coarser resolutions the simulated concentrations reach up to 5000 ppb for near-surface emission scenario.

350   The strongest peak of the whole measurement dataset was observed at the Estonian SMEAR station (EE-SMR) around 21Z 1.10 (Fig 8E1). The peak had a strong vertical gradient of methane ranging from about 200 ppb excess methane at 50 m above the ground reaching up to 1500 ppb at the 110 m height. The simulations show the arrival of a plume around the same time (Fig 8), but of much wider extent and of about 30-100 times lower intensity. The peak for the LoRes simulation had a similar vertical profile of the excess methane content: the 110 m level exhibits some 50 % higher values than the 90 m one.

The corresponding maps (Figs 9e, 10e, and 11e) show a plume in the vicinity of the station, however the concentrations there
355   do not exceed 100 ppb. Concentrated plumes with mixing ratios over 300 ppb and strong vertical inhomogeneity were found in the simulated fields some 100 km south-east of the EE-SMR station about one day earlier. The plumes were formed on 28.9 during stagnant conditions when the wind at the source location changed from eastern to western. Apparently this situation was not perfectly captured with the meteorological models, so the simulated trajectories and timings of the puff's movements got offset.

360   The arrival of the plume to the Zeppelin station (ZEP) at Spitsbergen archipelago was well reproduced by the model (Fig 8F), except for VHires simulation that did not cover the station. The resolution of the simulation had a moderate impact on the magnitude of the methane excess around the station (Figs10f, and 11f), and dual-peak structure of the timeseries was well reproduced at both resolutions. In both cases magnitude of the plume was slightly overestimated with FRP and underestimated with 5-km emission scenario.

7   Conclusions

365

With only the publicly available media reports, we were able to infer the temporal evolution and the injection height for the Nord Stream gas leaks in September 2022. The inventory specifies locations, vertical distributions and temporal evolutions of the methane sources. The inventory can be used to simulate the event with atmospheric transport models. The inventory is supplemented with a set of observational data tailored to evaluate the results of simulated atmospheric dispersion for the case.

370   Unlike in many cases of industrial accidents the total amount of methane released in the considered case is relatively well known and amounts to 3×110 kt of methane. The main uncertainties come from the assumption of gas composition in the pipes, and the assumption of 105 bar initial pressure in all damaged pipes. The fraction of methane We consider these figures are accurate within 10–15%.

In the present study we used a simplified model, assuming natural gas consisting of pure methane, so the total of our emission
375   inventory amounts $3x95$ kt. Sine the uncertainties of atmospheric dispersion models are larger

The case can be used to test and validate various source inversion techniques. The temporal and vertical distributions of the release have a significant impact on the simulated concentrations at the locations of the measurement sites.

The nature of a pollutant-transport problem with point sources and point receptors leaves very little chance to accurately predict the observation results. A transport model, even being perfect on its own, acts as an integrator for errors of the driving

380 meteorological model. A slight change in the plume location can lead to huge changes in the station timeseries extracted from the simulations. The timeseries are also substantially affected by the spatial resolution of the transport model. This sensitivity has to be accounted also in the inverse problems, where a slight variation of a model setup can substantially change the inversion setup.

Even with an accurate temporal profile, the effective injection height of the buoyant admixture has to be parameterised. An
385 attempt to use an existing parametrisation for wildfire plume injection height gave a notable improvement over a fixed injection profile. However, there is a substantial difference in mechanisms of buoyancy loss between an overheated moist plume from a fire and a methane plume: the fire plume loses buoyancy due to dilution, stable temperature stratification of the surrounding air and radiative cooling and gains buoyancy from the latent heat of water vapour condensation, whereas only dilution is relevant for the methane plume. Therefore a specially tailored plume-rise model would be more appropriate for the case. Nevertheless,
390 the FRP model was able to provide the evolution of the effective injection height for the methane plume that agrees with both LES simulations and the observations. The effect of the varying vertical injection profile should be accounted for when using the case for evaluating source-inversion techniques.

The evaluation of the simulation results against the station data and LES simulations suggests that the fire-plume injection profile was likely too low for the methane plume. The observed concentrations were between the two simulations with fixed
395 injection into the lowest 1500 m and lowest 5000 m. This gives an estimate for the actual injection heights for the gas leak. More insight into the effective vertical profile of the plume injection could be obtained from evaluating transport models against column-integrated observations with methane-observing satellites, e.g. IASI. This could be the subject for a future study.

Code and data availability. The code of SILAM model that can be used to reproduce the results of the current study is available from GitHub https://github.com/fmidev/silam-model/tree/v5_8_2 (Kouznetsov, 2023). Appendix also contains a code to simulate methane leak
400 from a pressurized pipe. The source estimates for the leak at 10-minute resolution together with the evaluated injection heights both in CSV format, and in Silam point-source format are available from the supplementary material. The summary of the observed and simulated station timeseries can be found in supplementary material.

Video supplement. The animation of the of the has plumes simulated with 0.02-deg resolution can be found from (Kouznetsov and Evgeny, 2023)

405 *Author contributions.* RK conceptualised the paper,performed the numerical simulations and evaluations, wrote the initial text and prepared the figures. MS contributed to the case conceptualization, participated in writing and editing of the manuscript, EK prepared the animation of the simulation results; MP adapted UCLALES for this study, performed the LES simulations and participated in analyzing their results, contributed to SILAM development, conceptualisation of the study, and editing the manuscript; RH and AU participated in Silam development, conceptualisation of the study, and editing the manuscript; YF assisted with literature overview and data mining. DK contributed to the

410 design of the conceptual model and to calculations for the gas leak; SN performed the measurements, provided the data for EE-SMR station and contributed to editing the manuscript; HJ performed the measurements and provided the data for EE-THK station.

Competing interests. The authors declare that no competing interests are present.

Disclaimer. The paper represents the authors' personal opinions and views, which might or might not agree with the positions of their organizations.

415 *Acknowledgements.* The study was funded by the EU Horizon project EXHAUSTION (grant 820655), FirEUrisk (grant 101003890) and NKS-B SOCHAOTIC project (contract AFT/B(22)1). Support of the Estonian Research Infrastructures Roadmap project Estonian Environmental Observatory (3.2.0304.11-0395), the Estonian Environmental Investment Support of Academy of Finland project 322532 (MOAC) for the LES modelling is acknowledged. Centre (KIK, grant no. 3-2.8/6574), the Estonian Research Council (project PRG1674) and the European Union's Horizon 2020 Research And Innovation programme (grant agreement no. 871115) ACTRIS IMP is kindly acknowledged.

References

Alvarez, R. A., Zavala-Araiza, D., Lyon, D. R., Allen, D. T., Barkley, Z. R., Brandt, A. R., Davis, K. J., Herndon, S. C., Jacob, D. J., Karion, A., Kort, E. A., Lamb, B. K., Lauvaux, T., Maasakkers, J. D., Marchese, A. J., Omara, M., Pacala, S. W., Peischl, J., Robinson, A. L., Shepson, P. B., Sweeney, C., Townsend-Small, A., Wofsy, S. C., and Hamburg, S. P.: Assessment of Methane Emissions from the U.S. Oil and Gas Supply Chain, Science, p. eaar7204, https://doi.org/10.1126/science.aar7204, 2018.

Briggs, G. A.: Plume Rise and Buoyancy Effects, in: Atmospheric Science and Power Production, edited by Andersson, D., p. 855, US Department of Energy, Germantown, Maryland, 1984.

Chen, X. and Zhou, T.: Negligible Warming Caused by Nord Stream Methane Leaks, Adv. Atmos. Sci., pp. s00 376–022–2305–x, https://doi.org/10.1007/s00376-022-2305-x, 2022.

Duncan, I. J.: Does Methane Pose Significant Health and Public Safety Hazards?—A Review, Environ. Geosci., 22, 85–96, https://doi.org/10.1306/eg.06191515005, 2015.

EPA: Inventory of {U.S.} Greenhouse Gas Emissions and Sinks: 1990–2015, Technical Report 430-P-17-001, United States Environmental Protection Agency, 2017.

Ferguson, S. A., Sandberg, D. V., and Ottmar, R.: Modelling the Effect of Landuse Changes on Global Biomass Emissions, in: Biomass Burning and Its Inter-Relationships with the Climate System, edited by Beniston, M., Innes, J. L., Beniston, M., and Verstraete, M. M., vol. 3, pp. 33–50, Springer Netherlands, Dordrecht, https://doi.org/10.1007/0-306-47959-1_3, 2000.

Freitas, S. R., Longo, K. M., Chatfield, R., Latham, D., Silva Dias, M. A. F., Andreae, M. O., Prins, E., Santos, J. C., Gielow, R., and Carvalho, J. A.: Including the Sub-Grid Scale Plume Rise of Vegetation Fires in Low Resolution Atmospheric Transport Models, Atmos. Chem. Phys., 7, 3385–3398, https://doi.org/10.5194/acp-7-3385-2007, 2007.

Hatakka, J. and Laurila, T.: ICOS ATC NRT CH4 growing time series, Utö - Baltic sea (57.0m), 2022-03-01–2022-10-16, https://hdl.handle.net/11676/yFO_L2onDwckHg_2194ej4Mx, 2022.

Heliasz, M. and Biermann, T.: ICOS ATC NRT CH4 growing time series, Hyltemossa (150.0m), 2022-03-01–2022-10-16, https://hdl.handle.net/11676/-uYDRenkp8mfYPJLhekmx9Ko, 2022.

Hõrrak, U., Salm, J., and Tammet, H.: Statistical Characterization of Air Ion Mobility Spectra at Tahkuse Observatory: Classification of Air Ions, J. Geophys. Res., 105, 9291–9302, https://doi.org/10.1029/1999JD901197, 2000.

Jia, M., Li, F., Zhang, Y., Wu, M., Li, Y., Feng, S., Wang, H., Chen, H., Ju, W., Lin, J., Cai, J., Zhang, Y., and Jiang, F.: The Nord Stream Pipeline Gas Leaks Released Approximately 220,000 Tonnes of Methane into the Atmosphere, Environmental Science and Ecotechnology, 12, 100 210, https://doi.org/10.1016/j.ese.2022.100210, 2022.

Kilkki, J., Aalto, T., Hatakka, J., Portin, H., and Laurila, T.: Atmospheric CO2 Observations at Finnish Urban and Rural Sites, Boreal Environment Research, 20 (2), 227–242, 2015.

Kim, J., Ryu, D., and Sovacool, B. K.: Critically Assessing and Projecting the Frequency, Severity, and Cost of Major Energy Accidents, The Extractive Industries and Society, 8, 100 885, https://doi.org/10.1016/j.exis.2021.02.005, 2021.

Kniebusch, M., Meier, H. M., Neumann, T., and Börgel, F.: Temperature Variability of the Baltic Sea Since 1850 and Attribution to Atmospheric Forcing Variables, J. Geophys. Res. Oceans, 124, 4168–4187, https://doi.org/10.1029/2018JC013948, 2019.

Kouznetsov, R.: Fmidev/Silam-Model: Release to Get DOI with Zenodo, Zenodo, https://doi.org/10.5281/ZENODO.7598284, 2023.

Kouznetsov, R. and Evgeny, K.: Methane dispersion form the Nord Stream gas leaks: Simulation with SILAM, driven with Harmonie meteorology, https://doi.org/10.5446/1770, 2023.

Kremens, R. L., Dickinson, M. B., and Bova, A. S.: Radiant Flux Density, Energy Density and Fuel Consumption in Mixed-Oak Forest Surface Fires, Int. J. Wildland Fire, 21, 722, https://doi.org/10.1071/WF10143, 2012.

Lehner, I. and Mölder, M.: ICOS ATC NRT CH4 growing time series, Norunda (100.0m), 2022-03-01–2022-10-16, https://hdl.handle.net/ 11676/DHD1wLPlqqb2Fo-NlWVBHed5, 2022.

Li, Y., Tong, D., Ma, S., Freitas, S. R., Ahmadov, R., Sofiev, M., Zhang, X., Kondragunta, S., Kahn, R., Tang, Y., Baker, B., Campbell, P., Saylor, R., Grell, G., and Li, F.: Impacts of Estimated Plume Rise on PM $_{2.5}$ Exceedance Prediction during Extreme Wildfire Events: A Comparison of Three Schemes (Briggs, Freitas, and Sofiev), Atmos. Chem. Phys., 23, 3083–3101, https://doi.org/10.5194/acp-23-3083-2023, 2023.

Lund Myhre, C., Platt, S. M., Hermansen, O., and Lunder, C.: ICOS ATC NRT CH4 growing time series, Zeppelin (15.0m), 2022-03-01–2022-10-16, https://hdl.handle.net/11676/jRuxDepDwdYIgT6bnMyS1Kb4, 2022a.

Lund Myhre, C., Platt, S. M., Lunder, C., and Hermansen, O.: ICOS ATC NRT CH4 growing time series, Birkenes (75.0m), 2022-03-01–2022-10-16, https://hdl.handle.net/11676/M1WVYeDMy6UtPnSvF6KKmq_L, 2022b.

Luts, A., Kaasik, M., Hõrrak, U., Maasikmets, M., and Junninen, H.: Links between the Concentrations of Gaseous Pollutants Measured in Different Regions of Estonia, Air Qual Atmos Health, 16, 25–36, https://doi.org/10.1007/s11869-022-01261-5, 2023.

Mollerup, J.: Measurement of the Volumetric Properties of Methane and Ethene at 310 K at Pressures to 70 MPa and of Propene from 270 to 345 K at Pressures to 3 MPa by the Burnett Method, The Journal of Chemical Thermodynamics, 17, 489–499, https://doi.org/10.1016/0021-9614(85)90148-X, 1985.

Noe, S. M., Niinemets, Ü., Krasnova, A., Krasnov, D., Motallebi, A., Kängsepp, V., Jõgiste, K., Hõrrak, U., Komsaare, K., Mirme, S., Vana, M., Tammet, H., Bäck, J., Vesala, T., Kulmala, M., Petäjä, T., and Kangur, A.: SMEAR Estonia: Perspectives of a Large-Scale Forest Ecosystem – Atmosphere Research Infrastructure, Forestry Studies, 63, 56–84, https://doi.org/10.1515/fsmu-2015-0009, 2015.

Nord Stream AG: Inline Inspection for the Nord Stream Pipeline, Background Information, Tech. rep., Nord Stream AG, 2013.

Poling, B. E., Prausnitz, J. M., and O'Connell, J. P.: The Properties of Gases and Liquids, McGraw-Hill, New York, 5th ed edn., 2001.

Rémy, S., Veira, A., Paugam, R., Sofiev, M., Kaiser, J. W., Marenco, F., Burton, S. P., Benedetti, A., Engelen, R. J., Ferrare, R., et al.: Two Global Data Sets of Daily Fire Emission Injection Heights since 2003, Atmospheric Chemistry and Physics, 17, 2921–2942, https://doi.org/10.5194/acp-17-2921-2017, 2017.

Sanderson, K.: What Do Nord Stream Methane Leaks Mean for Climate Change?, Nature, pp. d41 586–022–03 111–x, https://doi.org/10.1038/d41586-022-03111-x, 2022.

Sofiev, M., Vankevich, R., Lotjonen, M., Prank, M., Petukhov, V., Ermakova, T., Koskinen, J., and Kukkonen, J.: An Operational System for the Assimilation of the Satellite Information on Wild-Land Fires for the Needs of Air Quality Modelling and Forecasting, Atmospheric Chemistry and Physics, 9, 6833–6847, https://doi.org/10.5194/acp-9-6833-2009, 2009.

Sofiev, M., Ermakova, T., and Vankevich, R.: Evaluation of the Smoke-Injection Height from Wild-Land Fires Using Remote-Sensing Data, Atmos. Chem. Phys., 12, 1995–2006, https://doi.org/10.5194/acp-12-1995-2012, 2012.

Sofiev, M., Vira, J., Kouznetsov, R., Prank, M., Soares, J., and Genikhovich, E.: Construction of the SILAM Eulerian Atmospheric Dispersion Model Based on the Advection Algorithm of Michael Galperin, Geosci. Model Dev., 8, 3497–3522, https://doi.org/10.5194/gmd-8-3497-2015, 2015.

Stevens, B. and Seifert, A.: Understanding Macrophysical Outcomes of Microphysical Choices in Simulations of Shallow Cumulus Convection, Journal of the Meteorological Society of Japan, 86A, 143–162, https://doi.org/10.2151/jmsj.86A.143, 2008.

Stevens, B., Moeng, C.-H., and Sullivan, P. P.: Large-Eddy Simulations of Radiatively Driven Convection: Sensitivities to the Representation

495   of Small Scales, J. Atmos. Sci., 56, 3963–3984, https://doi.org/10.1175/1520-0469(1999)056<3963:LESORD>2.0.CO;2, 1999.

Stevens, B., Moeng, C.-H., Ackerman, A. S., Bretherton, C. S., Chlond, A., de Roode, S., Edwards, J., Golaz, J.-C., Jiang, H., Khairoutdinov, M., Kirkpatrick, M. P., Lewellen, D. C., Lock, A., Müller, F., Stevens, D. E., Whelan, E., and Zhu, P.: Evaluation of Large-Eddy Simulations via Observations of Nocturnal Marine Stratocumulus, Monthly Weather Review, 133, 1443–1462, https://doi.org/10.1175/MWR2930.1, 2005.

500 Tollefson, J.: Scientists Raise Alarm over 'Dangerously Fast' Growth in Atmospheric Methane, Nature, pp. d41 586–022–00 312–2, https://doi.org/10.1038/d41586-022-00312-2, 2022.

Venkatram, A. and Wyngaard, J. C.: Lectures on Air Pollution Modeling, American meteorological society, Boston, 1988.

Wooster, M. J., Roberts, G., Perry, G. L. W., and Kaufman, Y. J.: Retrieval of Biomass Combustion Rates and Totals from Fire Radiative Power Observations: FRP Derivation and Calibration Relationships between Biomass Consumption and Fire Radiative Energy Release, J.

505 Geophys. Res., 110, D24 311, https://doi.org/10.1029/2005JD006318, 2005.

Zabetakis, M. G.: Flammability Characteristics of Combustible Gases and Vapors, Tech. Rep. BM–BULL-627, 7328370, https://doi.org/10.2172/7328370, 1964.